WAVEFORM ANALYSIS TECHNIQUES IN AIRBORNE LASER SCANNING

W. Wagner [a], A. Roncat [a], T. Melzer [a], A. Ullrich [b]

[a] Christian Doppler Laboratory for Spatial Data from Laser Scanning and Remote Sensing, Institute of Photogrammetry and Remote Sensing, Vienna University of Technology, Gusshausstrasse 27-29, 1040 Wien, Austria
(ww, ar, tm)@ipf.tuwien.ac.at
[b] Riegl Research GmbH, 3580 Horn, Austria - aullrich@riegl.co.at

KEY WORDS: LIDAR, Waveform, Analysis, Pulse detection, Decomposition, Deconvolution, Point cloud

ABSTRACT:

Small-footprint airborne laser scanners with waveform-digitising capabilities are becoming increasingly available. Waveform-digitising is particularly advantageous when the backscattered echo waveform is complex because it allows selecting processing algorithms adjusted to the task. In addition, waveform-digitising laser scanners depict the physical measurement process in its entire complexity. This opens the possibility to derive the backscatter cross section which is a measure of the electromagnetic energy intercepted and reradiated by objects. In this paper approaches for deriving the cross section along the laser ray path are discussed. For data storage and processing reasons a practical approach is to model the waveform as the sum of a number of echoes backscattered from individual scatterers. This approach involves estimating the number of echoes, finding a match between the modelled echoes and the measured waveform, and estimating the cross section using calibration targets. For estimating the number and position of echoes the Average Square Difference Function (ASDF) method, which is a discrete time delay estimation technique, is tested. The results show that ASDF is a promising approach which appears to be less affected by noise compared to more traditional echo detection methods.

1. INTRODUCTION

Airborne laser scanning (ALS) is an optical measurement technique for obtaining information about the Earth's surface such as the topography of the land surface, the vegetation cover and the seafloor elevation in shallow waters. This technique is also often referred to as LIDAR, which stands for *LIght Detection And Ranging*. Most ALS instruments use pulse lasers, i.e. they send out short laser pulses in the visible and/or infrared part of the electromagnetic spectrum and measure some properties of the backscattered light to find range and/or other information of a distant target. While many of the first ALS systems provided only range information, ALS systems that digitise and record the complete echo waveform are becoming increasingly available.

Bathymetric lidar instruments designed for measuring depth of relatively shallow, coastal waters were the first full-waveform systems. These sensors transmit pulses at green wavelengths that penetrate several meters into the water depending on water clarity and turbidity. According to Wozencraft and Millar (2005) the maximum detectable depth of the seafloor is about 60 m. Scattering and spreading of the laser pulse at the air-water boundary, within the water column and the seafloor results in relatively complex echo waveforms (Tulldahl and Steinvall, 1999). Therefore, as Guenther et al. (2000) point out, it has not been possible to calculate all depths with high accuracy and reliability in real time during data acquisition. Precise depths are determined via post-flight processing of stored waveforms. More recently, NASA developed a small-footprint waveform-digitising bathymetric lidar that is also capable of mapping topography and vegetation (Wright and Brock, 2002). Nayeganhdi et al. (2006) demonstrate the capability of this sensor for depicting the vertical structure of vegetation canopies.

Also the echo waveform from vegetated areas is in general rather complex, in particular when the laser footprint is large (Sun and Ranson, 2000). Therefore also large-footprint airborne and spaceborne lidar systems designed for mapping of vegetation capture the complete echo waveform in order to allow the retrieval of geophysical parameters in post-processing. One of the airborne systems is the Laser Vegetation Imaging Sensor (LVIS) that transmits 10 ns long infrared pulses at repetition rates up to 500 Hz (Blair et al., 1999). Depending on flight altitude the footprint diameter is 1-80 m. So far, no satellite lidar system designed for the primary purpose of global vegetation mapping is available. However, the Geoscience Laser Altimeter System (GLAS) on-board of the ICESat satellite has acquired waveform data not only over the ice sheets but also over land surfaces. This will allow testing the usefulness of large-footprint (66 m) satellite-based waveform measurements for characterising forest structure and biomass (Harding and Carabajal, 2005).

For topographic mapping a small laser footprint and a high point density are required to collect a high number of geometrically well defined terrain echoes. Various filters that classify the echoes into terrain and off-terrain echoes based on purely geometric criteria can be used to reconstruct the terrain surface (Sithole and Vosselman, 2004). Given that this approach has worked well for lidar systems with ranging capabilities only, the need for waveform digitising lidar systems has not been evident for this application. Also, the benefit of waveform data for emerging ALS applications like 3D city modelling (Vosselman et al., 2005) and forest mapping (Hollaus et al., 2006) was not clear even though some early studies demonstrated the rich information content of small-footprint waveform data over land surfaces (Lin, 1997). Nevertheless, the first commercial waveform-digitising laser scanner system started appearing in the market in 2004. Even though research

$$P_r(t) = \sum_{i=1}^{N} \frac{D_r^2}{4\pi R_i^4 \beta_t^2} \eta_{sys} \eta_{atm} S(t) * \sigma_i(t) \qquad (2)$$

where N = number of targets
D_r = receiver aperture diameter
R_i = range from sensor to target i
η_{sys} = system transmission factor
η_{atm} = atmospheric transmission factor
β_t = transmitter beamwidth
σ_i = differential backscatter cross section of target i

Here, the waveform respectively cross section is represented by intermittent points irregularly distributed in 3D space (Figure 2). Neighbourhood relationships are not considered. An echo point is attributed a certain spatial dimension by adding the attribute "echo width". This approach is currently the standard in ALS processing.

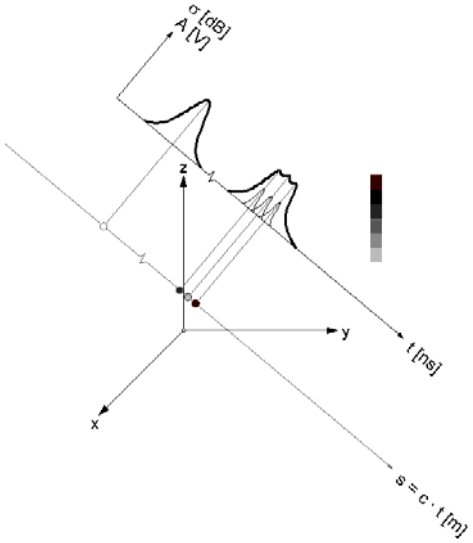

Figure 2. Discretisation of the ALS waveforms to obtain an irregularly distributed 3D point cloud. Here, the observed waveform is modelled explicitly as superposition of 3 Gaussian basis functions (targets).

2.3 Gaussian Decomposition

The decomposition of the waveform according to Eq. (2) becomes particularly simple, if both the individual cross sections and the emitted laser pulse can be described sufficiently well by Gaussian functions. In this case, the cross section can be computed in closed form using calibration targets (Wagner et al., 2006):

$$P_r(t) = \sum_{i=1}^{N} \hat{P}_i e^{-\frac{(t-t_i)^2}{2s_{p,i}^2}} \qquad (3)$$

$$\sigma_i = C_{Cal} R_i^4 \hat{P}_i s_{p,i} \qquad (4)$$

where $\hat{P}_i$ = amplitude of echo i
$s_{p,i}$ = width of echo i
t_i = round-trip time sensor to target i
C_{Cal} = calibration constant

Gaussian decomposition works by computing a nonlinear fit of the model Eq. (3) to the observed waveform. From the computed estimate (reconstruction), various target specific parameters such as echo width, intensity and position can be obtained. However, the number of targets as well as initial estimates for the distance of the targets have to be determined prior to the fit. This task is referred to as echo (pulse) detection.

Determining the number of echoes in ALS waveforms is not as simple as it may sound. Standard pulse detection methods such as *threshold*, *centre of gravity*, *maximum*, *zero crossing* of the second derivative, and *constant fraction* are discussed in Wagner et al. (2004). All these methods have their advantages and disadvantages. Problems occur when the waveforms have a complex shape and when the backscattered pulse is low compared to the noise level. In this case, advanced detection methods that minimise the influence of noise and account for non-ideal pulse forms should be sought. Thiel et al. (2005) tested a pulse correlation method and found almost no dependency on the signal to noise ratio. In our study we tested a time delay estimation technique as discussed in the next section.

3. ECHO DETECTION

For echo detection and time delay estimation, the *Average Square Difference Function* (ASDF) technique became relatively widespread during the last 15 years. Given two equidistantly sampled discrete time series, $x_1(t)$ and $x_2(t)$, the response value R of the ASDF is defined as (Jacovitti and Scarano, 1993):

$$R_{ASDF}(\tau) = \sum_{k=1}^{n} \left[x_1(kT) - x_2(kT + \tau) \right]^2 \qquad (5)$$

where T is the sampling interval and $(n\text{-}1)T$ the estimation window length. Figure 3 (bottom) shows a typical example of $R_{ASDF}(\tau)$. As one can see, this function is closely related to the well-known direct cross-correlation function but has some computational advantages (Jacovitti and Scarano, 1993). In the case of full-waveform analysis, the reference pulse $x_1(t)$ can be of any shape required by the respective task, e.g.

- the emitted laser pulse itself (see Figure 3, top)
- a Gaussian Pulse (see Figure 4) or
- a mean reference system waveform (see Figure 4) derived from a set of original laser pulses.

The time delay estimator Δt of a tentative echo is the value of τ corresponding to the minimum of $R_{ASDF}(\tau)$. In full-waveform laser scanning, one has to expect multiple echoes of a single laser pulse. Therefore, not only the global minimum, but also the local minima have to be taken into account. Tentative echoes are located between local maxima (depicted with black circles in Figure 5). Due to the fact that only positive values of R_{ASDF} appear and due to zero-padding outside the time window of x_2, the values of R_{ASDF} at the margins of its time window are always considered as local maxima (Figure 5). To distinguish real echoes from background noise, the detected minima must be separated from the neighbouring minima by a minimum distance ΔR_{min}. For our calculations we choose:

$$\Delta R_{\min} = 0.3\left(\max(R_{ASDF}(\tau)) - \min(R_{ASDF}(\tau))\right) \qquad (6)$$

Method	# detected echoes (%)				
	1	2	3	4	>= 5
Max-Detection	58,08	32,20	7,73	1,08	0,09
ASDF (Gaussian Pulse)	66,23	21,09	9,22	1,81	0,18
ASDF (Mean Reference Pulse)	65,89	20,65	9,74	2,01	0,24

Method	# detected echoes (%)				
	1	2	3	4	>= 5
Max-Detection	51,54	35,23	10,86	1,67	0,27
ASDF (Gaussian Pulse)	60,96	24,24	11,48	2,47	0,24
ASDF (Mean Reference Pulse)	60,64	23,63	12,15	2,70	0,27

Table 1. Number of Echoes computed with Max-Detection vs. ASDF-based Pulse Detection. Top: Sample 1 (Strip 2), bottom: Sample 2 (Strip 5).

From Table 1 one can learn that the used reference pulse of the ASDF-based techniques does not influence the results of pulse detection significantly. However, it is not clear if this is mainly a consequence of the scanner's recording system. Comparing max-detection with the ASDF-based methods, one can see that the latter are more likely to detect single echoes than max-detection. It appears that ASDF is less sensitive to laser ringing effects, which may be pronounced particularly after strong echoes (Nordin, 2006). On the other hand, Table 1 shows that it is also more likely to detect three and more echoes with an ASDF-based technique than with max-detection.

In the second experiment, the echo estimation of the three different methods (Gaussian Decomposition and the two ASDF-based approaches mentioned above) was compared. Two echoes computed with different estimation methods were treated as identical (one and the same) if their respective delays Δt did not differ more than the sampling interval of 1 ns (see Table 2).

Comparison	Identical echoes (%)		Median of difference [ns]		RMS of difference [ns]	
	Sample 1	Sample 2	Sample 1	Sample 2	Sample 1	Sample 2
Gaussian Decomposition / ASDF (Gauss.Pulse)	86,7	86,4	-0,0004	-0,0004	0,12	0,13
Gaussian Decomposition / ASDF (Mean Ref. Pulse)	86,9	86,8	0,0002	-7E-05	0,12	0,13
ASDF (Mean Ref. Pulse) / ASDF (Gauss.Pulse)	98,7	98,7	-0,0008	-0,001	0,05	0,05

Table 2. Comparison of Echo Estimation

The results of Table 2 show that in most cases (more than 85 %), classical pulse detection methods and ASDF-based approaches yield identical pulses. Also here, the two ASDF-variants show nearly identical results. Furthermore, it is given empirical evidence that in most cases echo estimation with Gaussian decomposition and with parabola fitting of the ASDF lead to comparable results since the medians of difference are very close to 0 and the standard deviations of difference are not greater than 0.15 ns. In metric dimensions, this would conform to 2.25 cm in the direction of the laser pulse which is a very low value in comparison to the ranges appearing in ALS.

5. CONCLUSIONS

The experiments presented in this paper give empirical evidence that both pulse detection and pulse estimation using the *Average Square Difference Function* (ASDF) method is a promising approach. To a high percentage, the results of ASDF-based techniques coincide with those achieved using standard methods. In these cases, it would not be necessary to determine the exact position of the echoes with non-linear fitting methods but could be done prior to Gaussian decomposition using the ADSF technique. This could accelerate the calculations, what is important given the increasingly large data volumes that novel laser scanner systems deliver. The remaining cases, where classical pulse detection methods and ASDF-based techniques do not coincide, need to be treated in more detail and are subject of further research.

6. REFERENCES

Blair, J. B., Rabine, D. L., and Hofton, M. A., 1999. The Laser Vegetation Imaging Sensor: a medium-altitude, digitisation-only, airborne laser altimeter for mapping vegetation and topography. *ISPRS Journal of Photogrammetry and Remote Sensing*, 54, pp. 115-122.

Doneus, M. and Briese, C., 2006. Digital terrain modelling for archaeological interpretation within forested areas using full-waveform laserscanning. In: M. Ioannides, D. Arnold, F. Niccolucci and K. Mania (Editors), The 7th International Symposium on Virtual Reality, Archaeology and Cultural Heritage VAST (2006), in press.

Guenther, G.C., Cunningham, G.C., LaRocque, P.E., and Reid, D.J., 2000. Meeting the accuracy challenge in airborne lidar bathymetry. In: *Proceedings of the EARSel-SIG-Workshop LIDAR*, Dresden, Germany, June 16-17, European Association of Remote Sensing Laboratories, 23 p.

Harding, D.J., and Carabajal, C.C., 2005. ICESat waveform measurements of within-footprint topographic relief and vegetation vertical structure. *Geophysical Research Letters*, 32, L21S10, pp. 1-4.

Hollaus, M., Wagner, W., Eberhöfer, C., and Karel, W., 2006. Accuracy of large-scale canopy heights derived from LiDAR data under operational constraints in a complex alpine environment. *ISPRS Journal of Photogrammetry and Remote Sensing*, 60(5), pp. 323-338.

Jacovitti, G., Scarano, G., 1993. Discrete Time Techniques for Time Delay Estimation. *IEEE Transactions on Signal Processing*, 41(2), pp. 525-533.

Jutzi, B., and Stilla, U., 2003. Laser pulse analysis for reconstruction and classification of urban objects. In: *International Archives of Photogrammetry and Remote Sensing*, Munich, Germany, 17-19. Sept., Vol. 34, Part 3/W8, pp. 151-156.

Jutzi, B., and Stilla, U., 2006. Range determination with waveform recording laser systems using a Wiener filter. *ISPRS Journal of Photogrammetry and Remote Sensing*, 61, pp. 95-107.

Kaasalainen, S., Ahokas, E., Hyyppä, J., and Suomalainen, J., 2005. Study of surface brightness from backscattered laser intensity: Calibration of laser data. *IEEE Geoscience and Remote Sensing Letters*, 2(3), pp. 255-259.